J. Fluid Mech. (2008), *vol.* 617, *pp.* 355–379.
doi:10.1017/S0022112008003935 Printed in the United Kingdom

Cellular vortex shedding in the wake of a tapered plate

VAGESH D. NARASIMHAMURTHY[1]†, HELGE I. ANDERSSON[1] AND BJØRNAR PETTERSEN[2]

[1]Fluids Engineering Division, Department of Energy and Process Engineering, Norwegian University of Science and Technology (NTNU), 7491 Trondheim, Norway
helge.i.andersson@ntnu.no

[2]Department of Marine Technology, NTNU, 7491 Trondheim, Norway
bjornar.pettersen@ntnu.no

(Received 18 December 2007 and in revised form 28 August 2008)

Direct numerical simulation (DNS) of vortex shedding behind a tapered plate with the taper ratio 20 placed normal to the inflow has been performed. The Reynolds numbers based on the uniform inflow velocity and the width of the plate at the wide and narrow ends were 1000 and 250, respectively. For the first time ever cellular vortex shedding was observed behind a tapered plate in a numerical experiment (DNS). Multiple cells of constant shedding frequency were found along the span of the plate. This is in contrast to apparent lack of cellular vortex shedding found in the high-Reynolds-number experiments by Gaster & Ponsford (*Aero. J.*, vol. 88, 1984, p. 206). However, the present DNS data is in good qualitative agreement with similar high-Reynolds-number experimental data produced by Castro & Watson (*Exp. Fluids*, vol. 37, 2004, p. 159). It was observed that a tapered plate creates longer formation length coupled with higher base pressure as compared to non-tapered (i.e. uniform) plates. The three-dimensional recirculation bubble was nearly conical in shape. A significant base pressure reduction towards the narrow end of the plate, which results in a corresponding increase in Strouhal number, was noticed. This observation is consistent with the experimental data of Castro & Rogers (*Exp. Fluids*, vol. 33, 2002, p. 66). Pressure-driven spanwise secondary motion was observed, both in the front stagnation zone and also in the wake, thereby reflecting the three-dimensionality induced by the tapering.

1. Introduction

It is a well-known fact that intrinsic three-dimensionalities arise in an initially two-dimensional flow when secondary instabilities are generated. This is the case for wakes of two-dimensional bluff bodies above a certain critical Reynolds number (Najjar & Vanka 1995; Williamson 1996; Najjar & Balachandar 1998). These three-dimensionalities can induce significant spanwise variations in the velocity and the pressure fields. In contrast, such three-dimensionalities may also occur due to extrinsic factors, such as the variation of the body shape (Gaster 1969; Piccirillo & Van Atta 1993; Vallès, Andersson & Jenssen 2002*a*, *b*; Narasimhamurthy, Andersson & Pettersen in press) or the boundary conditions (Maull & Young 1973; Parnaudeau *et al.* 2007). In his famous experimental study on slender cones Gaster (1969) found that even a small linear variation of the diameter along the span could

† Email address for correspondence: vagesh@ntnu.no

induce complex three-dimensionalities in the wake. Such linear variations of the local diameter imply a linear variation of the local Reynolds number along the span. Wakes of two-dimensional bluff bodies are inclined to maintain a surprisingly constant Strouhal number. On this basis one may envisage two different scenarios for how the local shedding frequency f will vary with the local diameter. Either f can vary continuously along the span so that the vortex filament is continuous and inclined with respect to the axis of the cylinder (the so-called oblique vortex shedding) or f can be constant only over a finite span so that the vortex filament is discontinuous (the so-called cellular vortex shedding). In fact, cellular vortex shedding was reported in both the experiments (Gaster 1969; Piccirillo & Van Atta 1993) and the computations (Vallès *et al.* 2002*b*; Parnaudeau *et al.* 2007; Narasimhamurthy *et al.* in press).

Following the successful findings of vortex dislocations or vortex splits in the wake of cones, Gaster & Ponsford (1984) went on to investigate the wakes of tapered and triangular plates at high Reynolds numbers ($Re = O(10^4)$) and over a range of taper ratios ($R_T = l/(d_2 - d_1)$, where l is the length of the plate and d_2 and d_1 denote the widths at the wide and narrow ends, respectively). They noticed that the pressure coefficient over the plate sections was not strictly two-dimensional and they therefore anticipated a weak secondary flow along the front stagnation line to be the most likely cause of this. In addition, they found a significant base pressure gradient along the span, driving the secondary flow from the wide end of the plate towards the narrow end. In spite of the strong three-dimensionalities observed, their hot-wire measurements failed to show any cellular vortex shedding. They concluded that the base Strouhal number was constant along the span in all their tapered models. The constancy of the Strouhal number implies that the shedding frequency varies inversely with the distance from the narrow end of the plate. In contrast, Maull & Young (1973) observed cellular shedding in the wake of a uniform (i.e. parallel-sided) plate with uniform shear as inflow. This motivated Castro & Rogers (2002) and Castro & Watson (2004) to carry out extensive hot-wire measurements in the wake of tapered and triangular plates of different taper and aspect ratios and with different end boundary conditions. The Reynolds numbers were still high ($Re = O(10^4)$). Surprisingly, they found end cells in those cases where the tip of the triangular plate was lying within the flow domain (free ends) and multiple cells of constant shedding frequency when the free ends were sealed with an end plate.

The laboratory experiments on tapered plates by Gaster & Ponsford (1984) and Castro & Watson (2004) were both at high Reynolds numbers and there is no evidence that cellular vortex shedding also occurs at low Reynolds numbers. It should be noted that turbulence at high Reynolds numbers has direct consequences on the vortex dynamics in the wake. Even though Castro & Rogers (2002) and Castro & Watson (2004) provided extensive spectral data, the detailed dynamics of the wake has not been explored so far. An in-depth and comprehensive study of the wake behind a tapered plate in general and at low Reynolds numbers in particular is therefore awaited. Direct numerical simulation (DNS) as a tool is the natural choice to explore such a complex wake structure, as it gives complete access to the instantaneous three-dimensional data. The above issues will be addressed for the first time in the present DNS study, where in addition to frequency analysis a more detailed investigation of the spanwise two-point correlations and the instantaneous vortical structures will be carried out. The spanwise variations of the velocity and the pressure fields will also be shown. First, however, results from a three-dimensional simulation of the steady flow past a tapered plate at very low Reynolds numbers are presented.

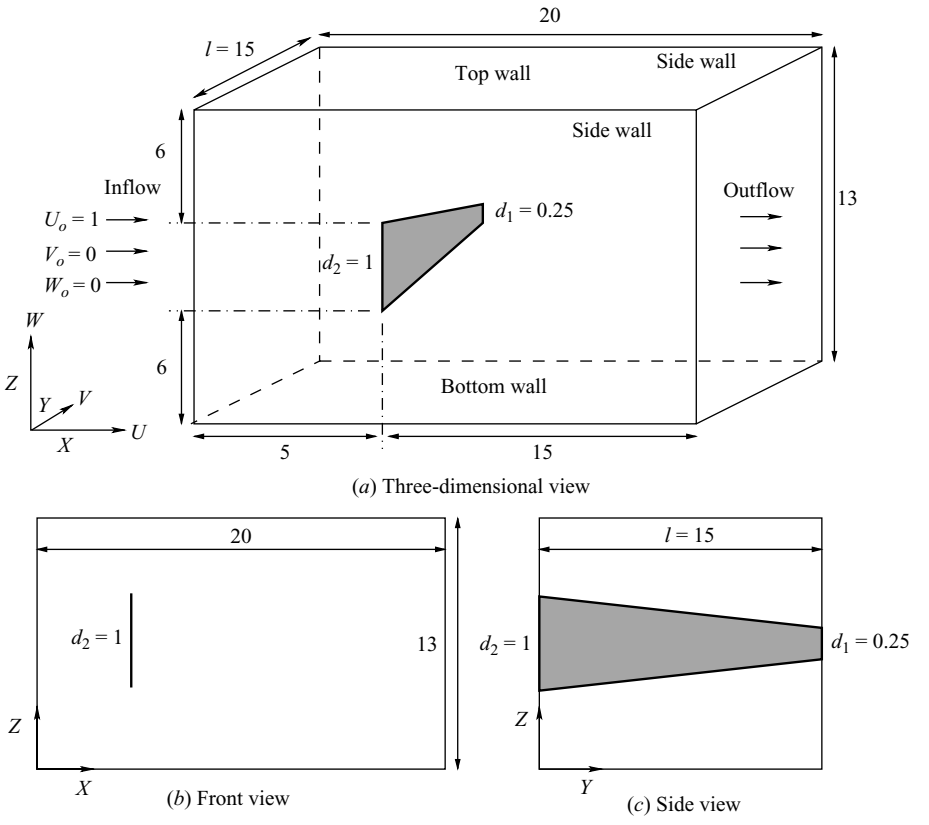

FIGURE 1. Computational domain (not to scale).

2. Formulation of the problem

Let us consider the flow past a tapered flat plate with the view to explore for the first time ever the vortex shedding at moderately high Reynolds numbers, i.e. lower than in the otherwise equivalent laboratory experiments but yet sufficiently high to make even the near-wake turbulent. The taper ratio is intentionally chosen to match one of the configurations studied by Castro & Watson (2004), whereas the Reynolds number is about two orders of magnitude lower than that in their experiment. Due to the substantial tapering, the local Reynolds number varies from 1000 at the wide end to 250 at the narrow end of the plate. It is evident from the existing literature that the first and second instability modes of three-dimensionality in the wake of uniform flat plates occur already at $Re = 105$–110 and $Re = 125$, respectively (Thompson, Leweke & Williamson 2001; Julien, Lasheras & Chomaz 2003; Julien, Ortiz & Chomaz 2004; Thompson *et al.* 2006). Thereby, the Reynolds number chosen in the present study is well above the transitional regime and the wake flow is expected to be turbulent over the entire span.

2.1. *Flow configuration and numerical method*

The computational domain was as shown in figure 1. All spatial dimensions are normalized by d_2 and all velocities are scaled with the uniform inflow velocity U_o. The mean width of the plate d_m was $0.625d_2$. The thickness of the plate was very small and equal to $0.02d_2$. The aspect ratio ($AR = l/d_m$), R_T and the Reynolds numbers Re_2, Re_1 and Re_m, based on the uniform inflow velocity U_o and the widths d_2, d_1 and d_m, respectively, are given in table 1.

Case	R_T	AR	Re_2	Re_m	Re_1
Steady laminar flow	20	24	20	12.5	5
Turbulent flow	20	24	1000	625	250
Castro & Watson (2004)	20	20	–	$>10^4$	–
Castro & Watson (2004)	20	15.4	–	$>10^4$	–
Castro & Watson (2004)	20	10	–	$>10^4$	–
Castro & Watson (2004)	20	5.8	–	$>10^4$	–
Gaster & Ponsford (1984)	18	–	–	$>10^4$	–

TABLE 1. Geometrical and flow parameters.

The Navier–Stokes (N-S) equations in incompressible form were solved in three-dimensional space and time using a parallel finite-volume code called MGLET (Manhart 2004; Narasimhamurthy *et al.* 2006). The code uses staggered Cartesian grid arrangements. Discretization of the spatial derivatives was achieved by means of a second-order central-differencing scheme. The time marching was carried out using a third-order explicit Runge–Kutta scheme for the momentum equations in combination with an iterative SIP (strongly implicit procedure) solver (Ferziger & Peric 1996) for the Poisson equation. The time step was chosen as $\Delta t = 0.001 d_2/U_o$ and the number of Poisson iterations per time step was limited to 30. Parallelization was implemented using message passing interface (MPI). The computations were performed on an IBM P575+ parallel computer.

The size of the computational domain in each coordinate direction was $L_x = 20d_2$, $L_y = 15d_2$ and $L_z = 13d_2$, as shown in figure 1. All three-dimensional simulations reported in this paper are for the same flow configuration and computational domain. The number of grid points in each coordinate direction ($N_x \times N_y \times N_z$) for the steady laminar flow case and the turbulent flow case was equal to $160 \times 150 \times 180$ and $320 \times 200 \times 200$, respectively. Non-equidistant grid spacings were used in the X–Z plane while an equidistant grid was used along the span (Y-direction). The ratio of grid size ΔZ near the plate's wide end to the local width of the plate, $\Delta Z/d_2$, is 0.01. This implies that the ratio of grid size near the plate's narrow end to the local width of the plate, $\Delta Z/d_1$, is 0.04. In order to justify that the present simulation is a fully resolved DNS, i.e. that all essential turbulent scales are captured, the grid size can be compared with Kolmogorov's microscale $\eta = (\nu^3/\varepsilon)^{1/4}$. Here, ε is the time-mean dissipation rate of fluctuating kinetic energy defined as

$$\varepsilon = \nu \left(\overline{\frac{\partial u_i}{\partial X_j}\frac{\partial u_i}{\partial X_j} + \frac{\partial u_i}{\partial X_j}\frac{\partial u_j}{\partial X_i}} \right) \approx \nu \left(\overline{\frac{\partial u_i}{\partial X_j}\frac{\partial u_i}{\partial X_j}} \right), \tag{2.1}$$

where u_i is the fluctuating part of the instantaneous velocity component which comprises both the unsteady fluctuations and the turbulent fluctuations. The contribution from the second term in the above definition of the total dissipation rate ε is negligible (Bradshaw & Perot 1993) and hence neglected in the present analysis. The grid size relative to the Kolmogorov microscale at some different spanwise locations at five different downstream positions are given in table 2 and compared with corresponding data for the plane wake DNS by Moser, Rogers & Ewing (1998) and the trailing-edge wake DNS of Yao *et al.* (2001). The data in table 2 show that the grid size in the present study is of the same order of magnitude as the local Kolmogorov length scale. The present grid resolution compares favourably with that used in other wake-flow simulations.

$X/d_{local} =$	1	3	5	8	12
Present DNS: $Re_{local} = 1000$	3.84	4.03	4.96	3.44	2.94
Present DNS: $Re_{local} = 750$	2.18	2.86	4.51	3.82	3.05
Present DNS: $Re_{local} = 500$	1.31	3.80	4.90	3.68	2.99
Yao *et al.* (2001)	6.88	5.07	3.42	2.76	2.44
Moser *et al.* (1998)			≈ 15		

TABLE 2. Grid resolution $\Delta\overline{X} = \Delta X/\eta$ values at various X/d_{local} positions measured from the axis of the plate.

Face	Boundary condition
Inflow	$U_o = 1; V_o = W_o = 0; \partial P/\partial X = 0$
Side walls	$V = 0; \partial U/\partial Y = \partial W/\partial Y = \partial P/\partial Y = 0$
Top and bottom walls	$W = 0; \partial U/\partial Z = \partial V/\partial Z = \partial P/\partial Z = 0$
Outflow	$\partial U/\partial X = \partial V/\partial X = \partial W/\partial X = 0; P = 0$

TABLE 3. Boundary conditions.

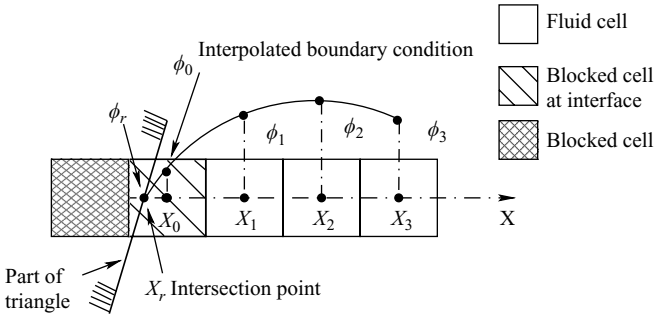

FIGURE 2. One-dimensional stencil configuration for interpolation in X-direction.

The boundary conditions used are as shown in table 3. A uniform velocity profile $U_o = 1$ was prescribed at the inlet without any free-stream perturbations and a Neumann boundary condition was used for the pressure. A free-slip boundary condition was applied on both the sidewalls, as well as at the top and bottom walls (cf. figure 1). At the outlet, a Neumann boundary condition was used for velocities and the pressure was set to zero.

A direct forcing immersed boundary method (IBM) (Narasimhamurthy *et al.* 2006; Peller *et al.* 2006) was used to transform the no-slip condition at the plate surface into internal boundary conditions at the nodes of the Cartesian grid (see Iaccarino & Verzicco 2003 and Mittal & Iaccarino 2005 for extensive reviews of different IBMs). The solid body (tapered plate) to be immersed in the Cartesian mesh was represented by a mesh consisting of triangles. The blocking of the Cartesian cells intersected by these triangles was accomplished as follows:

(i) The intersection points of a triangle surface and the coordinate line passing through the pressure cell centre were identified. The pressure cells containing those intersection points were blocked, as shown in figure 2.

(ii) In the second sweep all the pressure cells within the blocked surface were blocked.

(iii) Finally, all the velocity cells corresponding to blocked pressure cells were blocked.

Case	Blockage ratio	$Re = 10$	$Re = 20$
Present two-dimensional case	0.077	1.12	2.12
Smith (1985)		1.00	2.00
Hudson & Dennis (1985)		1.20	2.32
Ingham *et al.* (1991)		1.15	2.30
Dennis *et al.* (1993)	0.00	1.16	2.43
Dennis *et al.* (1993)	0.05	1.07	–
Dennis *et al.* (1993)	0.10	1.02	1.98
Dennis *et al.* (1993)	0.15	0.92	1.76
In *et al.* (1995)		1.24	2.60
Koumoutsakos & Shiels (1996)		–	2.10

TABLE 4. Non-dimensional length of the steady recirculation zone (L_w/d).

In figure 2, ϕ_o is the internal boundary condition value to be determined by interpolation. X_r is the intersection point between the triangle and the coordinate line. ϕ_r is the value at X_r which is known (the value on the wall). By considering the neighbouring variables ϕ_i (ϕ_1, ϕ_2, ϕ_3, etc.) the stencils are formed. A general stencil formulation for ϕ_o looks like

$$\phi_o = \left(\sum_{i=1}^{N} \alpha_i \phi_i \right) + \alpha_r \phi_r, \tag{2.2}$$

where N is the number of neighbouring cells involved in the interpolation. The interpolation coefficients α_i and α_r depend on the interpolation technique and geometry only and were therefore computed in a pre-processing step. In the present DNS study, we used least-squares interpolation of third-order accuracy. The detailed derivation, validation and implementation of this technique in the code MGLET were explained in Peller *et al.* (2006). Using matrix stability analysis they studied the numerical stability of higher-order Lagrange and least-squares interpolations and concluded that the least-squares interpolation of third-order is very robust and numerically stable. The stencil in each direction is one-dimensional. Weighting to account for three-dimensionality was employed by Tremblay, Manhart & Friedrich (2001).

2.2. *A two-dimensional case: the uniform plate*

Before undertaking the three-dimensional numerical simulations, benchmark two-dimensional calculations of the steady flow past a non-tapered plate placed normal to the free-stream were carried out. Two different simulations were performed with Reynolds number $Re = U_o d/\nu$ based on the uniform width d equal to 20 and 10. In both the simulations the domain size in X and Z directions was the same as that in the three-dimensional simulations (see figure 1). The number of grid points in each direction $N_x \times N_z$ were 140×100. The non-dimensional length of the steady recirculation zone (L_w/d) from the present simulations is in good agreement with the available experimental and numerical data (see table 4). Note the scatter among the earlier results, with differences of up to 30 % in estimating the length of the recirculating bubble. Koumoutsakos & Shiels (1996) attributed the differences between the existing simulations to the treatment of the boundary and far-field conditions. From their experiments Dennis *et al.* (1993) reported a strong dependence of the recirculation zone on the blockage ratio (see table 4). They performed experiments

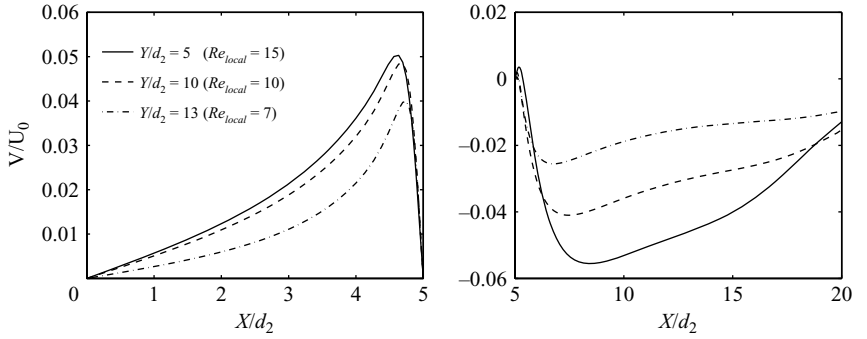

(*a*) Upstream the plate (*b*) Downstream the plate

FIGURE 3. Spanwise velocity V/U_o (secondary flow) at three different spanwise locations identified by the local Reynolds number $Re_{local} = U_o\ d/\nu$.

for different blockage ratios and obtained the bubble length for zero blockage by extrapolation. The substantial increase of L_w/d with decreasing blockage ratio is indeed noteworthy. It should be noted that small differences in the thickness of the plate might also have some influence on the steady separation bubble.

3. Results and discussion

3.1. *Steady laminar flow*

There is no doubt that random turbulence and quasi-organized vortex shedding will add complexities to the wake of a three-dimensional body. This motivates the need to first study the wake of a tapered plate in the absence of these two factors. One may speculate at this stage whether the wake flow behind a tapered plate can be considered as quasi-two-dimensional provided that the Reynolds number is lower than the critical value at which vortex shedding occurs. One may furthermore wonder how the secondary flow field, i.e. the departure from purely two-dimensional behaviour, will appear. In order to address these issues a steady laminar flow past a tapered plate was investigated (see table 1 for details). The numerical solution of the unsteady N-S equations converged to a steady state. The present three-dimensional calculation revealed a secondary spanwise velocity V, both in the front stagnation zone and in the wake of the plate (see figure 3). It can be observed from figure 3(*a*) that in the front stagnation zone the secondary flow is going from the wide end of the plate towards the narrow end, surprisingly as speculated by Gaster & Ponsford (1984) in their high-Reynolds-number study. On the contrary, the secondary motion on the rear side of the plate is rather complex. The flow in the immediate vicinity of the plate is going from the wide end towards the narrow end (see figure 3*b*). The variation of the base pressure coefficient $[C_p = 2(P - P_\infty)/(\rho U_o^2)$, where the reference pressure P_∞ is taken from the pressure at the inflow] along the span in figure 4 confirms the above observation. This is also in perfect agreement with the findings of Gaster & Ponsford (1984) at higher Reynolds number. The magnitude of this secondary flow is negligibly small, i.e. less than 0.5 % of the inflow velocity U_o. However, the direction of the secondary motion is reversed somewhat away from the plate where the flow goes from the narrow end of the plate towards the wide end. The magnitude of this spanwise velocity is typically of the order 5 % of the inflow U_o. The secondary motion in the spanwise direction is a direct consequence of three-dimensionality of

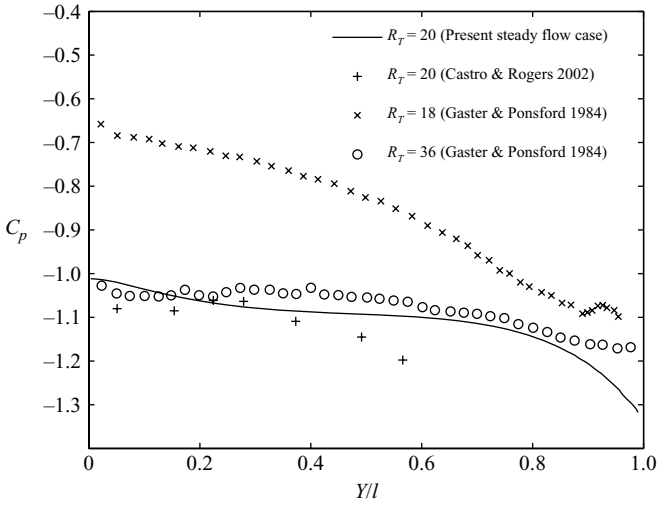

FIGURE 4. Base pressure coefficient variations along the span from the present steady laminar flow case and the previous experimental results at high Reynolds numbers.

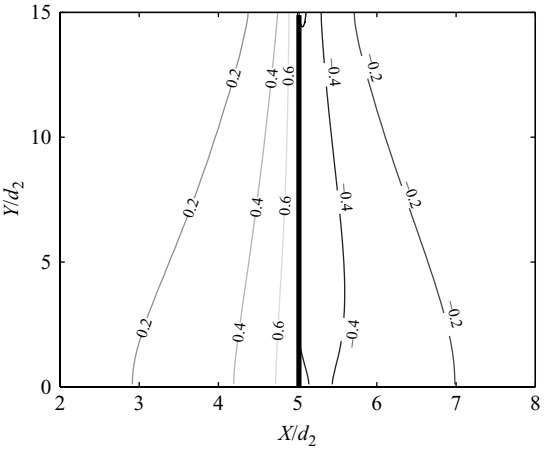

FIGURE 5. Pressure ($P/\rho\, U_o^2$) contours in the X–Y section plane through the axis of the plate in the steady laminar flow case. The plate is drawn as a bold line.

the tapered plate and this kind of secondary flow does not arise in the vicinity of a uniform plate.

The secondary flow is driven by a spanwise pressure gradient. The tapered plate introduces a variable blockage to the inflow along the span and this gives rise to a somewhat higher pressure near the wide end of the plate as compared to the narrow end. The pressure contours (isobars) in figure 5 show that the isobars are inclined to the stagnation line, thereby giving rise to a spanwise pressure gradient which drives the flow towards the narrow end. Similarly, the (negative) isobars in the wake are also tilted from the rear stagnation line, i.e. the lowest pressure is found in the wake downstream of the widest part of the plate. This observation indicates that the spanwise-oriented flow in the wake is also pressure-driven. The streamlines in X–Y plane cutting through the axis of the plate in figure 6 confirm the above observations.

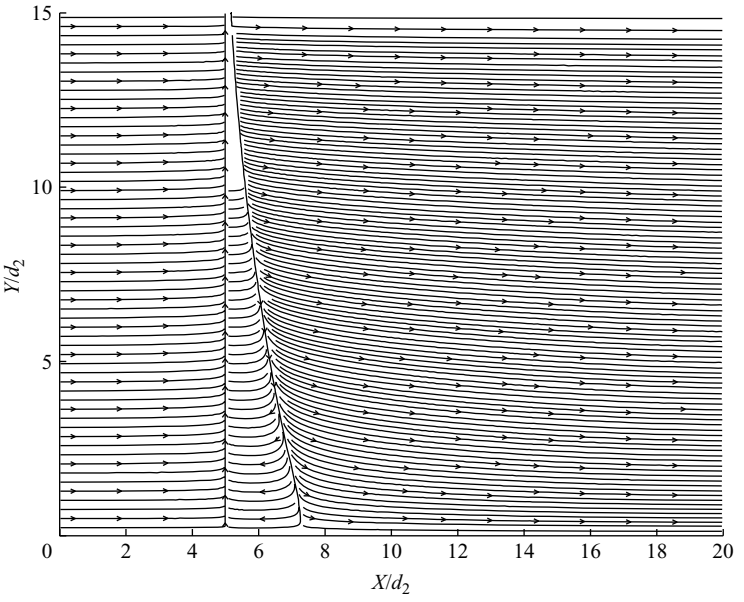

FIGURE 6. Streamlines in the $X-Y$ section plane through the axis of the plate illustrating the secondary flow direction and the recirculation zone in the steady laminar flow case. $Y/d_2 = 0$ corresponds to $Re_2 = 20$ and $Y/d_2 = 15$ corresponds to $Re_1 = 5$.

The constant length L_w of the closed wake behind a uniform plate is known to increase monotonically with the Reynolds number as long as the flow is in the steady laminar regime. Both the data from experiments by Dennis *et al.* (1993) and Ingham, Tang & Morton (1991) and computations by Hudson & Dennis (1985), In, Choi & Kim (1995) and others suggest this linear variation of L_w with the Re. In the present three-dimensional case, the wake length varies substantially along the span of the tapered plate. The wake behind the wide end is roughly 16 times longer than the wake behind the narrow end of the plate (see figure 6). If the local wake length L_w is scaled with the local plate width d_{local}, the spanwise variation of L_w/d_{local} shown in figure 7 is surprisingly close to the results for uniform or non-tapered (i.e. two-dimensional) plates. The deviation from two-dimensional behaviour is largest near the wide part of the tapered plate where the secondary flow is most pronounced (cf. figure 3). The results from the present simulation compare excellently with the data for uniform plates in the low-Re regime, i.e. along the narrow half of the plate.

3.2. *Turbulent flow*

3.2.1. *Wake pattern and frequency analysis*

The time evolution of the instantaneous velocity components U, V, W and the instantaneous pressure P was sampled along four lines parallel to the axis of the plate located $4d_m$, $8d_m$, $11d_m$ and $14d_m$ downstream the axis in X-direction, respectively. All lines were offset by $1d_m$ in Z-direction. It would be inappropriate to present all the data here because of space constraints. Therefore, only the time trace of the cross-stream velocity W sampled at $11d_m$ is shown in figure 8. The total sampling time was equal to $260d_2/U_o$ or $1040d_1/U_o$, which covers about 35 shedding cycles at the wide end and about 150 shedding cycles at the narrow end of the plate. Note that only half of the sampled data ($130d_2/U_o$) is shown in figure 8 for the

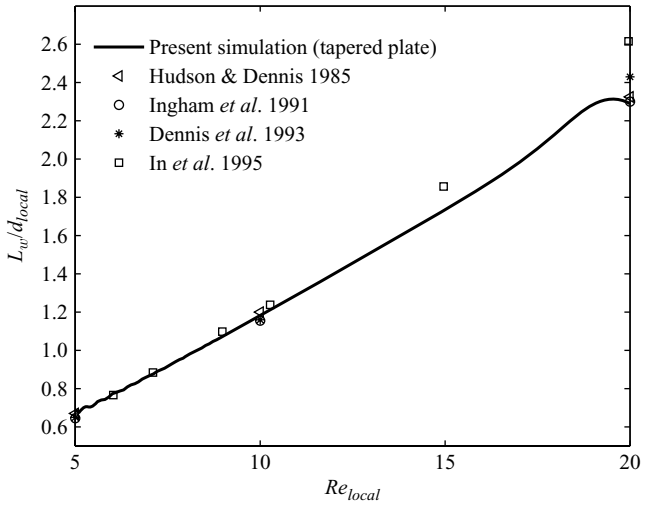

FIGURE 7. Non-dimensional length of the steady recirculation zone (L_w/d_{local}) versus local Reynolds number $Re_{local} = U_o\ d_{local}/\nu$. The symbols denote data for non-tapered plates with uniform width d.

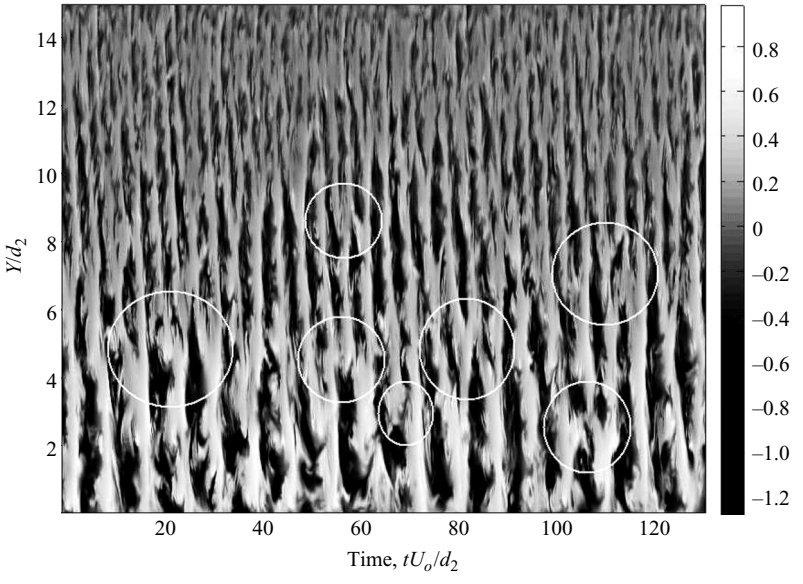

FIGURE 8. Time evolution of the cross-stream velocity (W) showing vortex-dislocations along the entire span (some marked by circles). The sampling line is at $X/d_m = 11$ and $Z/d_m = -1$ (measured from the axis of the plate). $Y/d_2 = 0$ corresponds to $Re_2 = 1000$ and $Y/d_2 = 15$ corresponds to $Re_1 = 250$.

purpose of clarity. The pattern clearly indicates oblique and cellular vortex shedding with random occurrence of vortex dislocations or vortex splits along the span. It is easy to see that the vortex dislocations are not occurring periodically in time at the same spanwise position. This justifies the need for such a long and expensive time sampling. Some time trace signals of the cross-stream velocity (W) at some different spanwise locations are shown in figure 9. Even though the turbulence signatures are chaotic, a low-frequency modulation, a typical feature of vortex dislocations, is

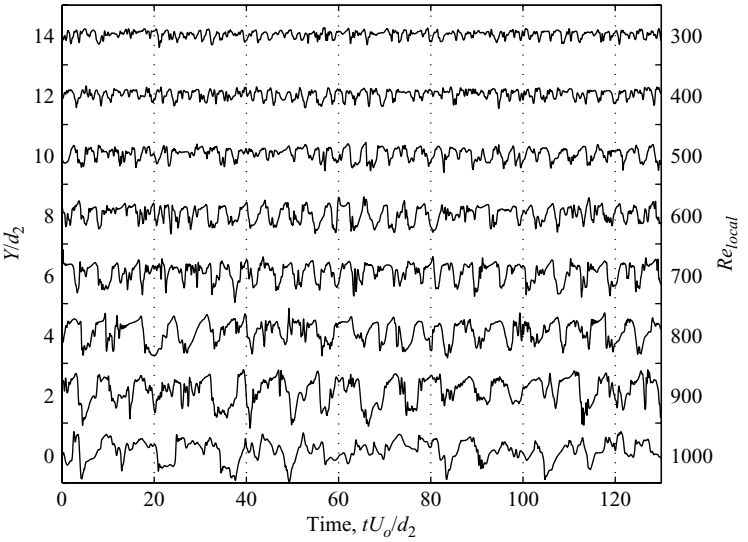

FIGURE 9. Time traces of the cross-stream velocity (W) at different spanwise locations.

visible in certain signals. The signal at $Y/d_2 = 4$ in figure 9, for instance, shows a low-frequency signature at time $tU_o/d_2 \approx 17$, which corresponds to the vortex dislocation at $Y/d_2 \approx 4$ in figure 8. Such low-frequency fluctuations were also observed in the wake of uniform circular cylinders, first by Roshko (1954) in the transition regime and later Bloor (1964) suggested that these low-frequency irregularities reflect the presence of three-dimensionalities that would render the flow turbulent as it travels downstream. Williamson (1992) attributed these low-frequency irregularities in the transition regime to the presence of large-scale spot-like vortex dislocations. The dislocations were found to be generated during the changeover of eddy shedding mode from laminar to mode A (Williamson 1996). Thereby there exists some firm evidence that low-frequency signatures can be associated with vortex dislocations even for parallel-sided bluff bodies. However, this is not always true. The low-frequency signatures observed by Najjar & Vanka (1995), Najjar & Balachandar (1998) and Wu *et al.* (2005) in the wake of uniform flat plates were rather differently interpreted. While Najjar & Vanka (1995) speculated the low-frequency behaviour to be due to a low-frequency flapping of the shear layer, Najjar & Balachandar (1998) attributed the phenomenon to the gradual variation of the flow between two regimes: a regime of short formation region and a regime of long formation region. They observed that in the short formation regime the shear layer rolls up closer to the plate to form coherent spanwise vortices, while in the long formation regime the shear layer extends farther downstream and the rolled-up Kármán vortices are less coherent. Similar regimes leading to low-frequency modulations were also noticed at higher Reynolds numbers by Wu *et al.* (2005).

To enable quantitative comparisons the frequency spectra were obtained by Fourier analysis of cross-stream velocity (W) time traces. A sample spectrum is shown in figure 10, which is taken at the mid-span of the plate ($Re_{local} = 625$) and is provided in a double-logarithmic plot. The primary shedding frequency corresponds to the most energetic frequency which is found at $fd_2/U_o = 0.2257$. This gives the local Strouhal number, defined as $St_{local} = fd_{local}/U_o = 0.1411$. Shedding frequencies ($f$) obtained from the fast Fourier transform of the velocity signals are plotted against the local widths of the plate in figure 11. Note that the shedding frequency is not

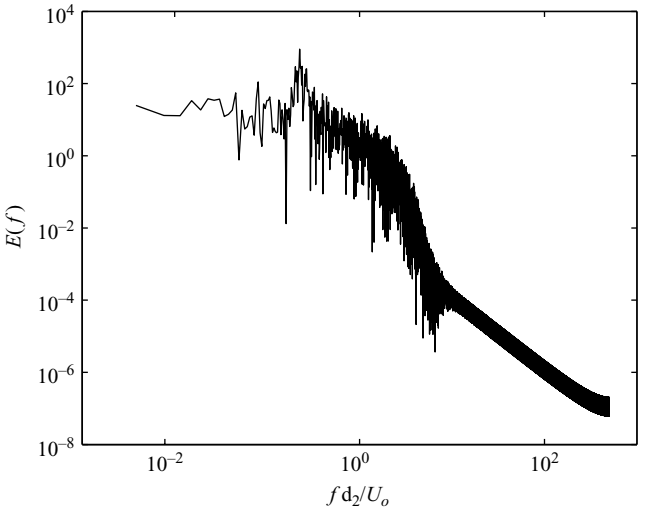

FIGURE 10. Spectrum for the mid-span location $Y/d_2 = 7.5$ ($Re_{local} = 625$).

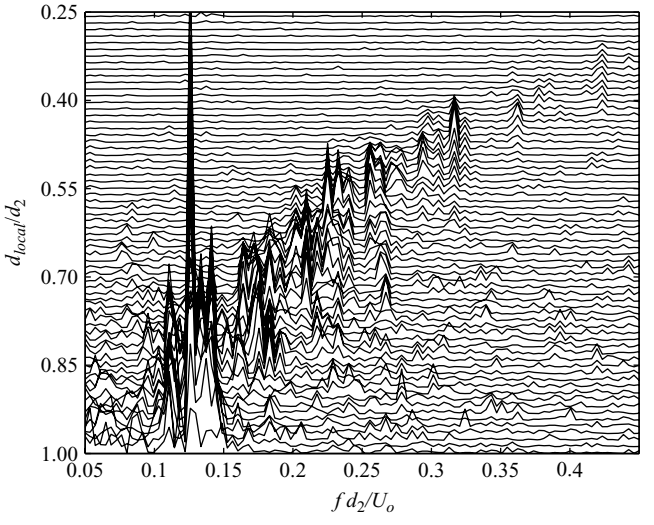

FIGURE 11. Shedding frequencies ($f d_2/U_o$) from Fourier analysis versus d_{local}.

varying continuously along the span but in discrete steps between cells of constant shedding frequency. This is in contrast to what Gaster & Ponsford (1984) found at high Reynolds numbers, where they reported an almost constant value of base Strouhal number $f d_2/U_o$ along the span. The local Strouhal number St_{local} is plotted against d_{local} in figure 12. It seems like the width of the constant shedding frequency cells increases with the d_{local}, an effect is also observed in the wake of tapered cylinders (Piccirillo & Van Atta 1993; Narasimhamurthy *et al.* 2006; Parnaudeau *et al.* 2007; Narasimhamurthy *et al.* in press). The same observation can also be made from the results of Castro & Watson (2004) in figure 13. Here, the variation of the St_{local} from the present DNS study is compared against their experimental data. Note that the taper ratio is the same in both the cases (see table 1). In spite of the different Reynolds numbers the qualitative agreement is striking. The structure of

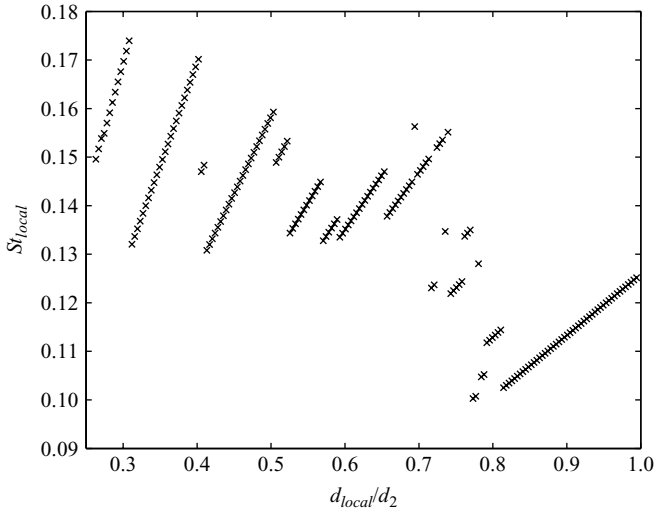

FIGURE 12. Local Strouhal number St_{local} versus local width of the plate d_{local}.

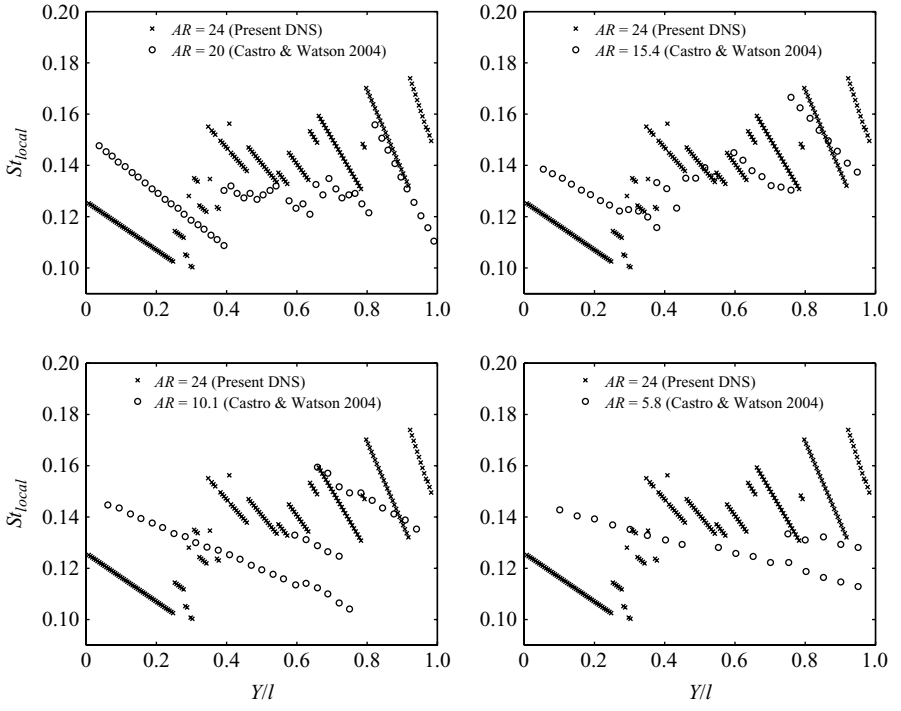

FIGURE 13. Local Strouhal number St_{local} from the present DNS calculation plotted against the hot-wire measurements data by Castro & Watson (2004) along the entire span. Taper ratio $R_T = 20$ is same in both the cases. $Y/l = 0$ corresponds to $Re_2 = 1000$ and $Y/l = 1$ corresponds to $Re_1 = 250$.

the vortex shedding is strongly dependent on the aspect ratio for low aspect ratios. The local Strouhal number behaviour deduced from the hot-wire measurements of Castro & Watson (2004) shows only a minor difference between their aspect ratios, $AR = 15.4$ and $AR = 20$. We are therefore inclined to infer that the impact of the

aspect ratio difference between the present DNS study ($AR = 24$) and the Castro & Watson (2004) data for $AR = 20$ is negligibly small.

3.2.2. *Spanwise two-point correlation*

It is clear from the preceding section that cellular vortex shedding exists in the wake of a tapered plate even at low Reynolds numbers. To further explore this cellular vortex shedding phenomenon, the spanwise coupling of the vortex motion is studied by means of spanwise two-point correlation, where the correlation coefficient is defined as $\overline{\phi(Y)\phi(Y+\Delta Y)}/\overline{\phi(Y)^2}$. In statistically homogeneous flows, this correlation is a function only of the separation ΔY between the two points and does not depend on the position Y. In addition, the correlation is symmetric in the direction of homogeneity, i.e. independent of the sign of ΔY. However, this should not be true in the present case as the flow is inhomogeneous in all the three directions. This is indeed what we see in figures 14 and 15. The correlation coefficient of the secondary flow (V) is plotted against the spanwise separation ΔY at three different positions, $Y/d_2 = 5, 7.5$ and 10 in figures 14(a), 14(b) and 14(c), respectively. The correlation is clearly asymmetric and the secondary motion remains surprisingly correlated almost for the entire span. However, it is interesting to see that the correlation reduces to $\approx 20\,\%$ within $\Delta Y = 1d_2$. The negative correlation towards the narrow end of the plate implies that the secondary motion is oppositely directed at that position. This is clearly an end effect as it appears only over $1d_2$ at the narrow end. The correlation coefficient is also computed for the cross-stream velocity (W) component (see figure 15). This coefficient is again asymmetric. However, it is not surprising that the correlation goes to zero within $\Delta Y = 3d_2$, since the cross-stream velocity is directly linked to the spanwise vorticity and the spanwise vortex filaments experience random vortex dislocations along the span.

3.2.3. *Instantaneous vortical structures*

In order to identify the topology of the vortex cores correctly the definition of λ_2 by Jeong & Hussain (1995) was used. λ_2 corresponds to the second largest eigenvalue of the symmetric tensor $\boldsymbol{S}_{ij}\boldsymbol{S}_{ij} + \boldsymbol{\Omega}_{ij}\boldsymbol{\Omega}_{ij}$, where $\boldsymbol{S}_{ij}$ and $\boldsymbol{\Omega}_{ij}$ are respectively the symmetric and anti-symmetric parts of the velocity gradient tensor. Iso-surfaces of negative λ_2 and pressure ($P/\rho\ U_o^2$) at the same instant in time are shown in figures 16 and 17, respectively. The snapshots clearly demonstrate the discontinuity in the spanwise vortex filament at $Y/d_2 \approx 5, 9$ and 12.5. As seen in figure 17, the three-dimensional recirculation bubble is nearly conical in shape. This observation is consistent with the finding of Gaster & Ponsford (1984) reported from their high-Reynolds-number experiments. Figures 18(a) and 18(b) show the iso-surfaces of instantaneous streamwise and cross-stream vorticity components at the same instant in time. Vortices rotating in opposite directions are distinguished by colour (white and black). The vortices towards the narrow part of the plate ($Y \rightarrow 15$) appear to be organized but highly irregular in the very near wake and rapidly break up into incoherent motion downstream. Towards the wider part of the plate ($Y \rightarrow 0$) there is chaos even in the near wake. This is obviously a Reynolds number effect. The above observation is clearly illustrated in figure 19, where $-\lambda_2$ at two different spanwise positions were plotted in the X–Z plane perpendicular to the plate. Note that the shear layer extends farther downstream of the plate before rolling-up than in the case of parallel-sided plates (e.g. Najjar & Vanka 1995 and Najjar & Balachandar 1998). This is consistent with the conclusion drawn by Gaster & Ponsford (1984), where they noticed that tapered plates have longer formation length than their corresponding uniform plates.

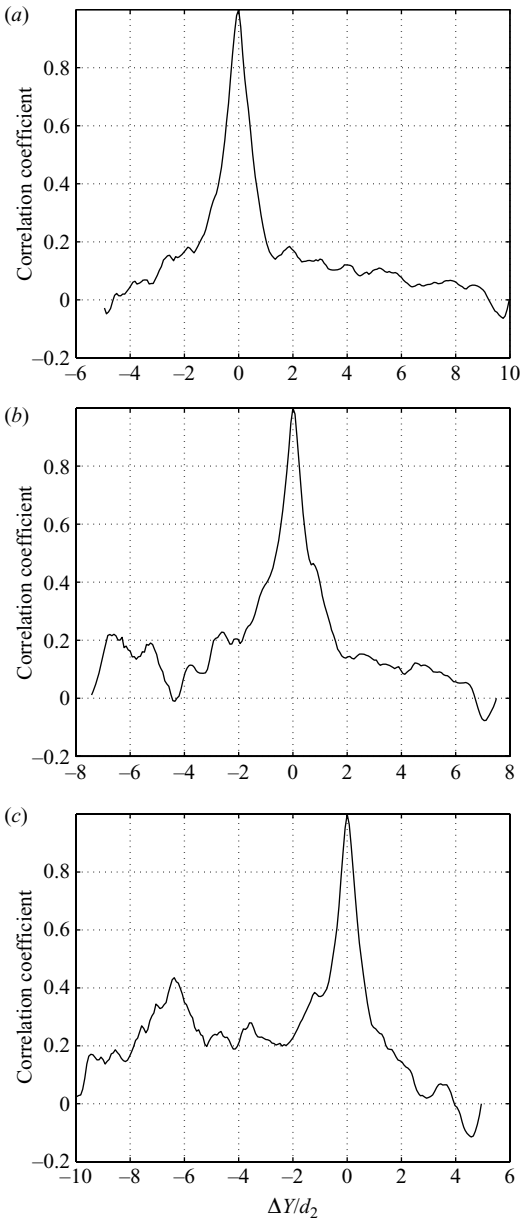

FIGURE 14. Spanwise correlation of the secondary flow (V) at three different positions along the span corresponding to the Re_{local}: (*a*) 750; (*b*) 625; (*c*) 500. ΔY corresponds to spanwise separation length.

3.2.4. *Mean pressure and base suction coefficients*

Time-averaged statistical quantities were evaluated by sampling for $170d_2/U_o$ or $680d_1/U_o$ time units. This sampling period corresponds to about 60 mean shedding cycles. One sample is taken every tenth time step for averaging.

The mean pressure coefficient is defined as $\overline{C}_p = 2(\overline{P} - P_\infty)/(\rho U_o^2)$, where the reference pressure P_∞ is taken from the pressure at the inflow. The distribution of $\overline{C}_p$ on the surface of the tapered plate at different spanwise positions is compared

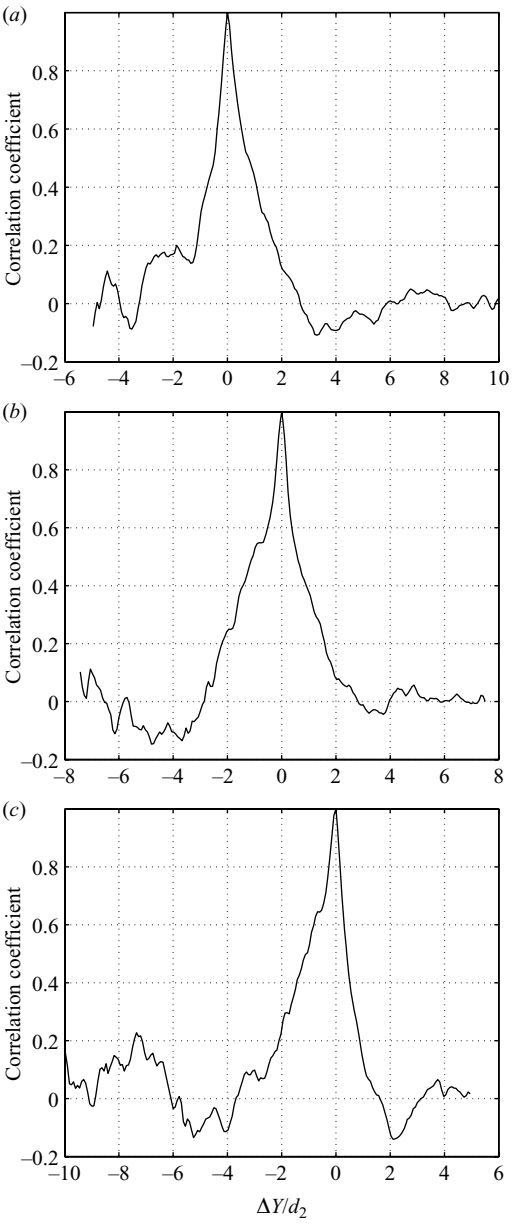

FIGURE 15. Spanwise correlation of the cross-stream (W) velocity at three different positions along the span corresponding to the Re_{local}: (*a*) 750; (*b*) 625; (*c*) 500. ΔY corresponds to spanwise separation length.

against uniform plate results in figure 20. The pressure on the upstream surface of the tapered plate compares well with the uniform plate experimental data by Fage & Johansen (1927) and the numerical data by Najjar & Vanka (1995) and Najjar & Balachandar (1998). It should be noticed that the front face pressures collapse if plotted versus Z/d_{local} rather than Z/d_2. The constancy of the pressure in the base region is well captured in the present DNS study. However, the pressure in the base region is significantly higher compared to the uniform plate data. The reason for this

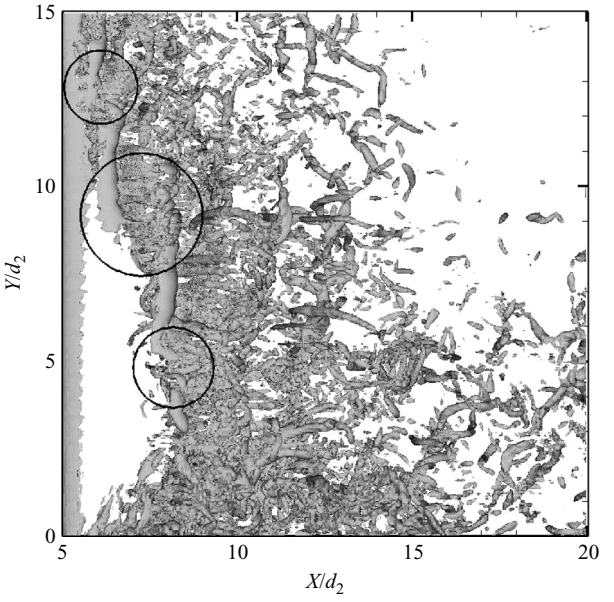

FIGURE 16. $-\lambda_2$ vortical structures at time $t = 130\ d_2/U_o$ showing vortex-dislocations along the span at $Y/d_2 \approx 5, 9, 12.5$ (marked by circles). The flow direction is from left to right and the Y-axis corresponds to the axis of the plate.

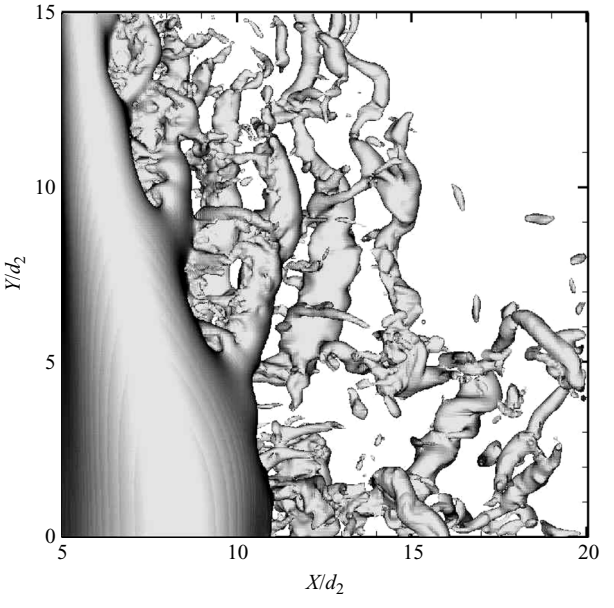

FIGURE 17. Three-dimensional iso-pressure ($P/\rho\ U_o^2 = -0.07$) contours at time $t = 130\ d_2/U_o$ showing vortex-dislocations along the span at $Y/d_2 \approx 5, 9, 12.5$. The flow direction is from left to right and the Y-axis corresponds to the axis of the plate.

lies in the wake formation length, which is closely coupled to the local base pressure. As discussed already in the previous section, Gaster & Ponsford (1984) reported very strong and periodic vortex shedding behind the uniform plates, which gives rise to significantly shorter formation lengths compared to tapered plates. Najjar & Vanka

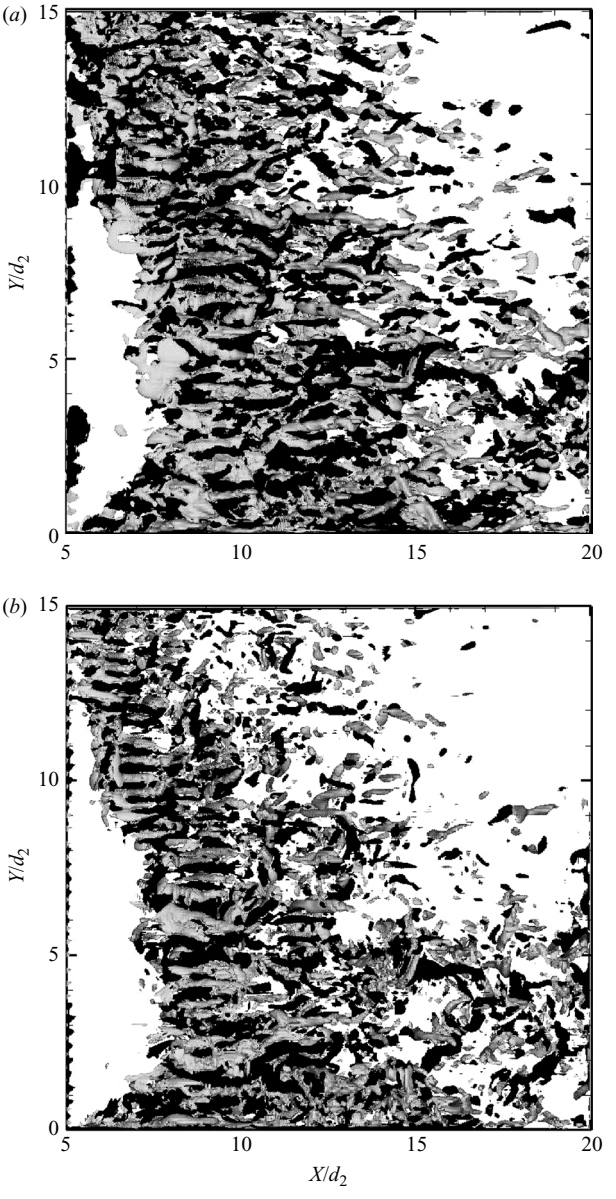

FIGURE 18. Three-dimensional iso-surfaces at the same time instant, $t = 130\ d_2/U_o$. (*a*) Streamwise vorticity, ω_x. (*b*) Cross-stream vorticity, ω_z. The flow direction is from left to right and the Y-axis corresponds to the axis of the plate. The surfaces coloured white and black mark $\omega\nu/U_o^2 = -0.002$ and $\omega\nu/U_o^2 = +0.002$, respectively.

(1995) noted that the wake formation length in their uniform plate case at $Re = 1000$ was about two plate widths. The mean wake formation length in the present case in figure 21 clearly shows that at $Re_{local} = 1000$ the bubble is six times the local plate width, i.e. three times larger than in the corresponding uniform plate case. This suggests a coupling between the local base pressure and the vortex formation process (Bearman 1965, 1967).

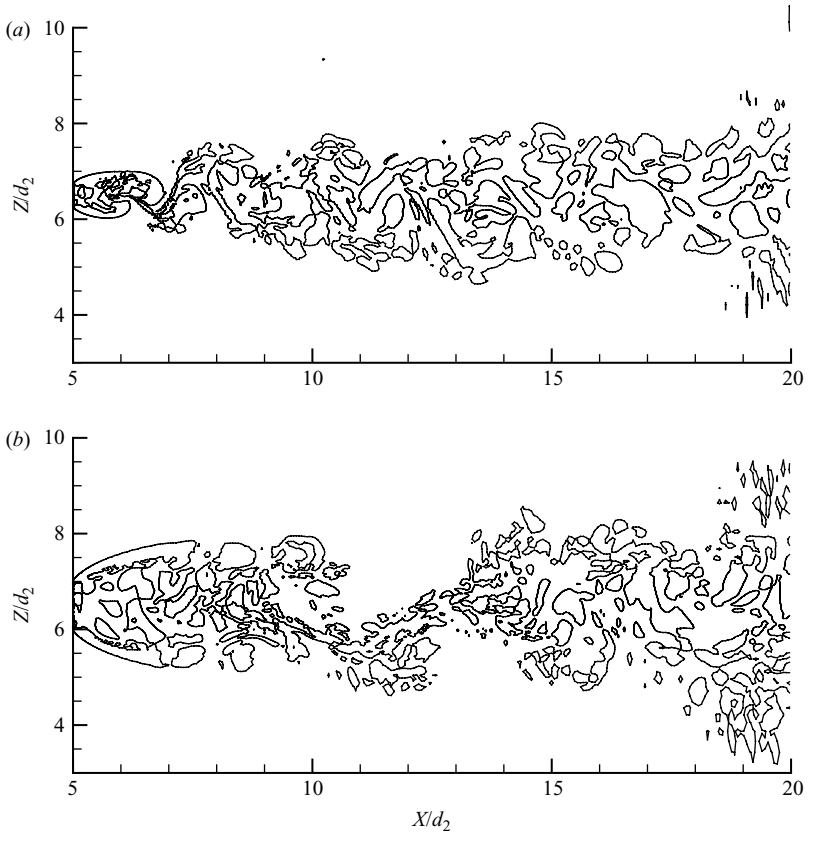

FIGURE 19. Contour plots of $-\lambda_2$ at two different spanwise positions: (*a*) $Y/d_2 = 12$; (*b*) $Y/d_2 = 2$.

The mean base pressure coefficient along the span of the plate is shown in figure 22. Even though Gaster & Ponsford (1984) observed base pressure variations for all their tapered models with a significant reduction towards the narrow end of the plate, they did not give any explanation to this phenomenon. They noticed, however, that this base pressure gradient was driving the secondary flow from the wide end of the plate towards the narrow end. Castro & Rogers (2002) made a similar observation in their experiments and they attributed this reduction in base pressure towards the narrow end to the corresponding increase in Strouhal number. By comparing the $\overline{C}_p$ variations in figure 22 to the St_{local} variation in figure 13, the present DNS data confirms the conclusion given by Castro & Rogers (2002).

3.2.5. *Secondary motion*

The pressure-driven secondary motion in the steady laminar flow regime has been discussed in § 3.1. There is also some evidence in experiments (Gaster & Ponsford 1984; Castro & Rogers 2002) that such pressure-driven secondary flow may exist even at high Reynolds numbers, i.e. in the turbulent flow regime. This issue has not yet been thoroughly addressed. The present turbulent flow simulation revealed a mean spanwise velocity $\overline{V}$, both in the front stagnation zone and also in the wake of the plate (see figure 23). It can be observed from figure 23(*a*) that in the front stagnation zone the secondary flow is still going from the wide end of the plate towards the

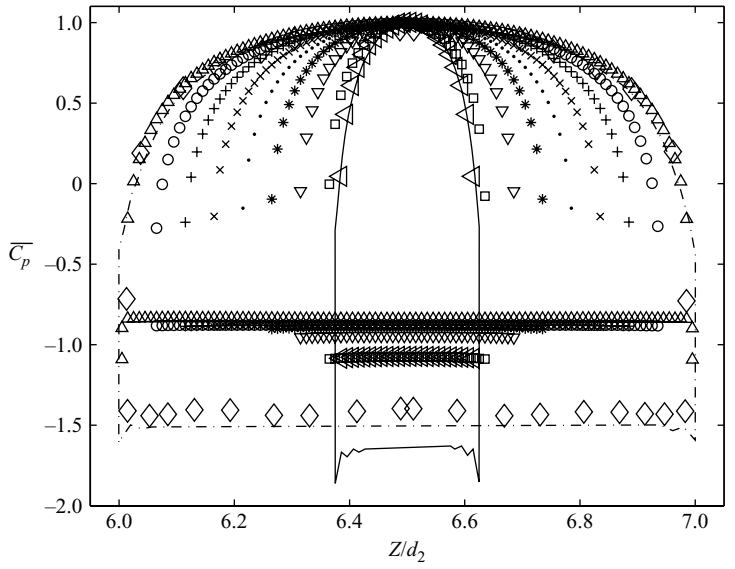

FIGURE 20. Distribution of the mean pressure coefficient, $\overline{C}_p$, on the surface of the plate from the present DNS (tapered plate): △, $Y/d_2 = 0$; ○, $Y/d_2 = 2$; +, $Y/d_2 = 4$; ×, $Y/d_2 = 6$; ●, $Y/d_2 = 8$; ∗, $Y/d_2 = 10$; ∇, $Y/d_2 = 12$; □, $Y/d_2 = 14$; ◁, $Y/d_2 = 15$; and the experimental data (uniform plate) of Fage & Johansen (1927): ⋄, $Re = 1.5 \times 10^5$; and the DNS results (uniform plate) of Najjar & Vanka (1995): —.—, $Re = 1000$; Najjar & Balachandar (1998): —, $Re = 250$.

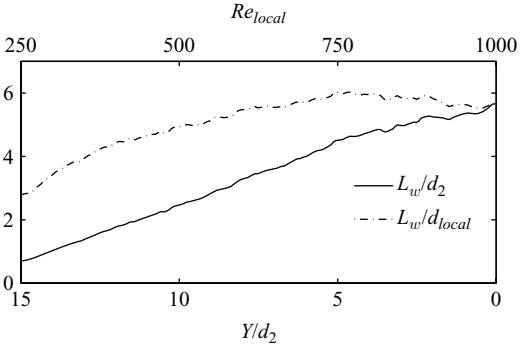

FIGURE 21. Non-dimensional length of the mean recirculation zone versus Re_{local}. L_w is the streamwise distance from the axis of the plate to the position where the mean streamwise velocity $\overline{U}$ changes sign from negative to positive.

narrow end, similar to what we saw in the steady laminar regime (cf. figure 3*a*) and also as speculated by Gaster & Ponsford (1984). The magnitude of this spanwise velocity is around 10 % of the inflow U_o, i.e. twice larger than what we observed in the steady laminar regime. On the contrary, the secondary motion on the rear side of the plate in figure 23(*b*) is more complex and similar to what we observed in the steady laminar wake (see figure 3*b*). The flow in the near vicinity of the plate is going from the wide end towards the narrow end. This is in perfect agreement to what Gaster & Ponsford (1984) claimed in their experimental study. However, the direction of this secondary motion is surprisingly reversed somewhat away from the plate, so that the flow goes from the narrow end of the plate towards the wide end.

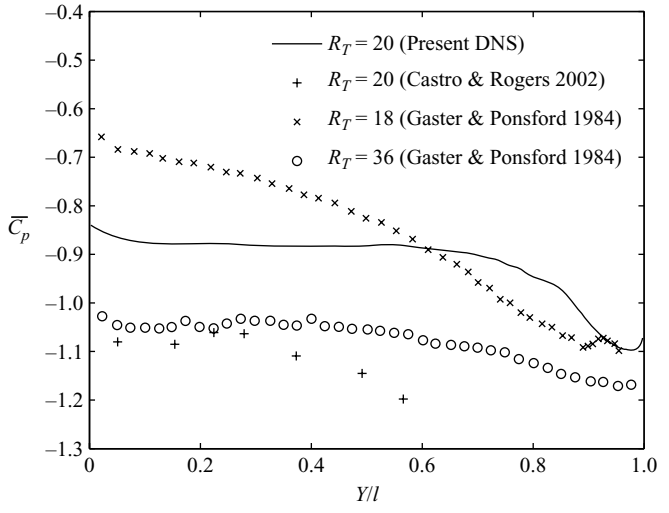

FIGURE 22. Mean base pressure coefficient variations along the span for different taper ratios from the present turbulent flow case and experiments.

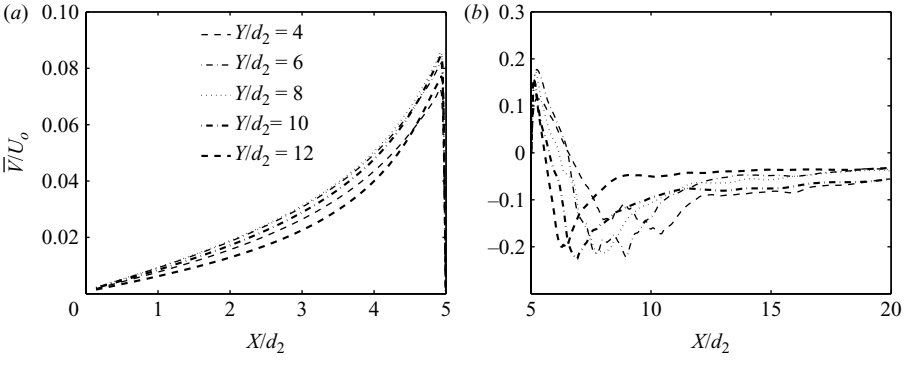

FIGURE 23. Time-mean spanwise velocity (secondary flow) at different spanwise locations: (*a*) upstream the plate and (*b*) downstream the plate.

The magnitude of this spanwise velocity is around 20 % of the inflow U_o, i.e. about four times larger than what was observed in the steady laminar regime (cf. figure 3*b*). The secondary motion discussed above is driven by local pressure gradients. Mean pressure profiles at different spanwise locations in figure 24(*a*) and the isobars in figure 24(*b*) justify the above claim. The streamlines in $X-Y$ plane through the axis of the plate in figure 25 confirm the above observations. The streamlines within the separation bubble are distinctly different from those in the steady laminar case (figure 6). The shape of the -0.4 mean–pressure contour in figure 24(*b*) resembles the topology of the instantaneous iso-pressure surface in figure 17.

4. Conclusions

For the first time ever cellular vortex shedding has been observed behind a tapered plate in a numerical experiment (DNS). Frequency analysis, two-point correlations and three-dimensional visualizations collectively confirm that multiple cells of constant

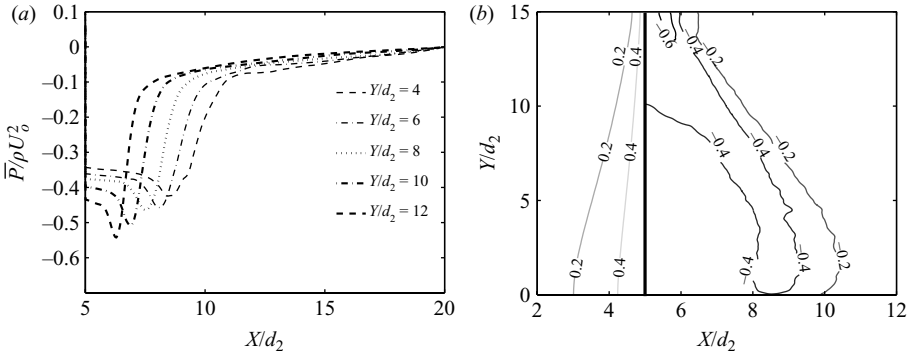

FIGURE 24. (*a*) Mean pressure ($\overline{P}/\rho U_o^2$) in the wake at different spanwise locations. (*b*) Iso-bars in the $X-Y$ section plane through the axis of the plate. The plate is drawn as a bold line.

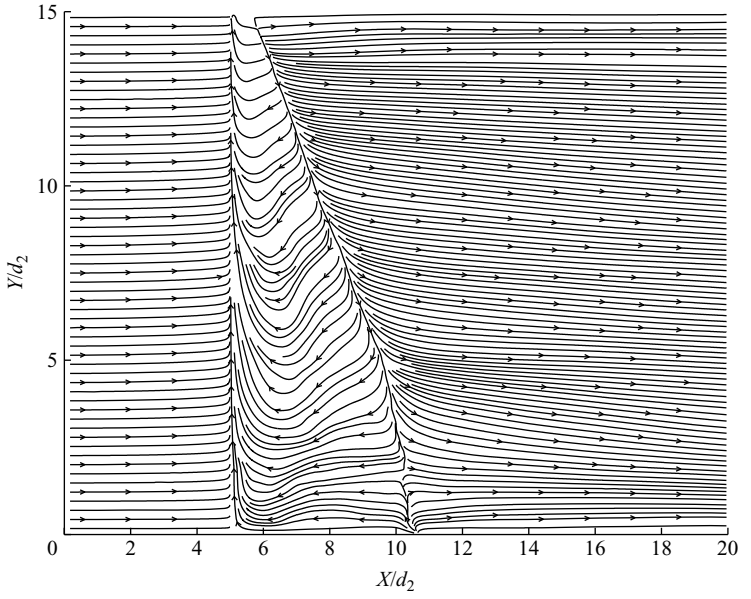

FIGURE 25. Streamlines in the $X-Y$ section plane through the axis of the plate illustrating the mean secondary flow ($\overline{V}$) direction and the mean recirculation zone.

shedding frequency exist along the span of the plate. This is in contrast to apparent lack of cellular vortex shedding found in the high-Reynolds-number experiments by Gaster & Ponsford (1984). However, the present DNS data is in good qualitative agreement with similar high-Reynolds-number experimental data produced by Castro & Rogers (2002) and Castro & Watson (2004). A possible reason for the failure of Gaster & Ponsford (1984) experiments to show cellular vortex shedding was suggested by Castro & Rogers (2002). They argued that tracking of the variation in shedding frequency across the span certainly requires closely spaced measurements, whereas only a modest number of spectral measurements were made by Gaster & Ponsford (1984).

In the present DNS study, it has been observed that tapering tends to decorrelate the vortex shedding both in time and also along the span. The decorrelated vortex

shedding results in a longer formation length of the separation bubble and higher base pressure as compared to the non-tapered (i.e. uniform) plates. This is consistent with the conclusion drawn by Gaster & Ponsford (1984). Base pressure variations were noted in the present tapered configuration with a significant reduction towards the narrow end of the plate. This reduction in base pressure towards the narrow end results in a corresponding increase in Strouhal number. This observation is consistent with the findings of Castro & Watson (2004).

The three-dimensional recirculation bubble was found to be nearly conical in shape in both the steady laminar case and the turbulent flow case. This observation is similar to what Gaster & Ponsford (1984) reported in their high-Reynolds-number experiment. In addition it was observed that the length of the closed wake in the steady laminar case is in good agreement with non-tapered (i.e. uniform) plate data. Thus the flow field in planes perpendicular to the plate axis can be considered as quasi-two-dimensional in the steady laminar flow regime.

The present three-dimensional calculations revealed a pressure-driven spanwise secondary motion, both in the steady laminar flow regime and also in the turbulent flow regime. It was observed that in the front stagnation zone the secondary flow is going from the wide end of the plate towards the narrow end. This is in accordance with the speculations by Gaster & Ponsford (1984) in their high-Reynolds-number study. On the contrary, the secondary flow pattern on the rear side of the plate is rather complex. The flow in the immediate vicinity of the plate is going from the wide end towards the narrow end. This is in perfect agreement to what Gaster & Ponsford (1984) claimed. However, the direction of this secondary motion is surprisingly reversed somewhat away from the plate, so that the flow goes from the narrow end of the plate towards the wide end. The spanwise secondary motion was found to be more pronounced in the turbulent flow case than in the steady laminar case.

The present computer simulations of flow past a linearly tapered plate facilitated detailed study of three-dimensional wake flow phenomena in the laminar and low-Reynolds-number turbulent flow regime, which thereby supplement earlier experimental investigations at substantially higher Reynolds numbers. Similarities and differences between the two distinctly different cases herein and the earlier high-*Re* studies are pointed out. The cellular shedding observed at relatively low *Re* in the present study supports and complements the findings of Castro & Watson (2004) at a significantly higher Reynolds number.

The authors are grateful for the constructive comments from the anonymous reviewers and to Professor I. P. Castro (Southampton, UK) who encouraged us to undertake this study and also provided some helpful suggestions. This work has received support from The Research Council of Norway (Programme for Supercomputing) through a grant of computing time. The first author was the recipient of a research fellowship offered by The Research Council of Norway.

REFERENCES

Bearman, P. W. 1965 Investigation of the flow behind a two-dimensional model with a blunt trailing edge and fitted with splitter plates. *J. Fluid Mech.* **21**, 241–255.

Bearman, P. W. 1967 The effect of base bleed on the flow behind a two-dimensional model with a blunt trailing edge. *Aero. Q.* **18**, 207.

Bloor, M. S. 1964 The transition to turbulence in the wake of a circular cylinder. *J. Fluid Mech.* **19**, 290–304.

Bradshaw, P. & Perot, J. B. 1993 A note on turbulent energy dissipation in the viscous wall region. *Phys. Fluids* A **5**, 3305–3306.

Castro, I. P. & Rogers, P. 2002 Vortex shedding from tapered plates. *Exp. Fluids* **33**, 66–74.

Castro, I. P. & Watson, L. 2004 Vortex shedding from tapered, triangular plates: taper and aspect ratio effects. *Exp. Fluids* **37**, 159–167.

Dennis, S. C. R., Wang, Q., Coutanceau, M. & Launay, J. L. 1993 Viscous flow normal to a flat plate at moderate Reynolds numbers. *J. Fluid Mech.* **248**, 605–635.

Fage, A. & Johansen, F. C. 1927 On the flow of air behind an inclined flat plate of infinite span. *Br. Aero. Res. Coun. Rep. Memo.* **1104**, 81–106.

Ferziger, J. H. & Peric, M. 1996 *Computational Methods for Fluid Dynamics*. Springer.

Gaster, M. 1969 Vortex shedding from slender cones at low Reynolds numbers. *J. Fluid Mech.* **38**, 565–576.

Gaster, M. & Ponsford, P. J. 1984 The flows over tapered flat plates normal to the stream. *Aero. J.* **88**, 206–212.

Hudson, J. D. & Dennis, S. C. R. 1985 The flow of a viscous incompressible fluid past a normal flat plate at low and intermediate Reynolds numbers: the wake. *J. Fluid Mech.* **160**, 369–383.

Iaccarino, G. & Verzicco, R. 2003 Immersed boundary technique for turbulent flow simulations. *Appl. Mech. Rev.* **56**, 331–347.

In, K. M., Choi, D. H. & Kim, M.-U. 1995 Two-dimensional viscous flow past a flat plate. *Fluid Dyn. Res.* **15**, 13–24.

Ingham, D. B., Tang, T. & Morton, B. R. 1991 Steady two-dimensional flow past a normal flat plate. *J. Appl. Math. Phys. (ZAMP)* **42**, 584–604.

Jeong, J. & Hussain, F. 1995 On the identification of a vortex. *J. Fluid Mech.* **285**, 69–94.

Julien, S., Lasheras, J. & Chomaz, J.-M. 2003 Three-dimensional instability and vorticity patterns in the wake of a flat plate. *J. Fluid Mech.* **479**, 155–189.

Julien, S., Ortiz, S. & Chomaz, J.-M. 2004 Secondary instability mechanisms in the wake of a flat plate. *Eur. J. Mech. B/Fluids* **23** (1), 157–165.

Koumoutsakos, P. & Shiels, D. 1996 Simulations of the viscous flow normal to an impulsively started and uniformly accelerated flat plate. *J. Fluid Mech.* **328**, 177–227.

Manhart, M. 2004 A zonal grid algorithm for DNS of turbulent boundary layers. *Comput. Fluids* **33**, 435–461.

Maull, D. J. & Young, R. A. 1973 Vortex shedding from bluff bodies in a shear flow. *J. Fluid Mech.* **60**, 401–409.

Mittal, R. & Iaccarino, G. 2005 Immersed boundary methods. *Annu. Rev. Fluid Mech.* **37**, 239–261.

Moser, R. D., Rogers, M. M. & Ewing, D. W. 1998 Self-similarity of time-evolving plane wakes. *J. Fluid Mech.* **367**, 255–289.

Najjar, F. M. & Balachandar, S. 1998 Low-frequency unsteadiness in the wake of a normal flat plate. *J. Fluid Mech.* **370**, 101–147.

Najjar, F. M. & Vanka, S. P. 1995 Effects of intrinsic three-dimensionality on the drag characteristics of a normal flat plate. *Phys. Fluids* **7**, 2516–2518.

Narasimhamurthy, V. D., Andersson, H. I. & Pettersen, B. (in press) Direct numerical simulation of vortex shedding behind a linearly tapered circular cylinder. In *Proc. IUTAM Symposium on Unsteady Separated Flows and Their Control*. Springer, Heidelberg.

Narasimhamurthy, V. D., Schwertfirm, F., Andersson, H. I. & Pettersen, B. 2006 Simulation of unsteady flow past tapered circular cylinders using an immersed boundary method. In *Proc. ECCOMAS Computational Fluid Dynamics* (ed. J. Périaux, P. Wesseling & E. Oñate). TU Delft.

Parnaudeau, P., Heitz, D., Lamballais, E. & Silvestrini, J. H. 2007 Direct numerical simulations of vortex shedding behind cylinders with spanwise linear nonuniformity. *J. Turbul.* **8**(13), 1–13.

Peller, N., Le Duc, A., Tremblay, F. & Manhart, M. 2006 High-order stable interpolations for immersed boundary methods. *Intl J. Num. Meth. Fluids* **52**, 1175–1193.

Piccirillo, P. S. & Van Atta, C. W. 1993 An experimental study of vortex shedding behind linearly tapered cylinders at low Reynolds number. *J. Fluid Mech.* **246**, 163–195.

Roshko, A. 1954 On the development of turbulent wakes from vortex streets. *Tech. Rep.* 1191. NACA.

Smith, F. T. 1985 On large-scale eddy closure. *J. Math. Phys. Sci.* **19**, 1.

Thompson, M. C., Hourigan, K., Ryan, K. & Sheard, G. J. 2006 Wake transition of two-dimensional cylinders and axisymmetric bluff bodies. *J. Fluids Struct.* **22**, 793–806.

Thompson, M. C., Leweke, T. & Williamson, C. H. K. 2001 The physical mechanism of transition in bluff body wakes. *J. Fluids Struct.* **15**, 607–616.

Tremblay, F., Manhart, M. & Friedrich, R. 2001 DNS and LES of flow around a circular cylinder at a subcritical Reynolds number with cartesian grids. In *LES of Complex Transitional and Turbulent Flows*, pp. 133–150. Kluwer Academic Publishers.

Vallès, B., Andersson, H. I. & Jenssen, C. B. 2002*a* Direct-mode interactions in the wake behind a stepped cylinder. *Phys. Fluids* **14**, 1548–1551.

Vallès, B., Andersson, H. I. & Jenssen, C. B. 2002*b* Oblique vortex shedding behind tapered cylinders. *J. Fluids Struct.* **16**, 453–463.

Williamson, C. H. K. 1992 The natural and forced formation of spot-like dislocations in the transition of a wake. *J. Fluid Mech.* **243**, 393–441.

Williamson, C. H. K. 1996 Vortex dynamics in the cylinder wake. *Annu. Rev. Fluid Mech.* **28**, 477–539.

Wu, S. J., Miau, J. J., Hu, C. C. & Chou, J. H. 2005 On low-frequency modulations and three-dimensionality in vortex shedding behind a normal plate. *J. Fluid Mech.* **526**, 117–146.

Yao, Y. F., Thomas, T. G., Sandham, N. D. & Williams, J. J. R. 2001 Direct numerical simulation of turbulent flow over a rectangular trailing edge. *Theor. Comput. Fluid Dyn.* **14**, 337–358.